Study of Selective Laser Melting for Bonding of 304L Stainless Steel to Grey Cast Iron

Baily Thomas, Austin Sutton, Ming C. Leu
Department of Mechanical and Aerospace Engineering, Missouri University of Science and Technology, Rolla, MO 65409

Baily Thomas, Austin Sutton, Dr. Ming Leu
Missouri University of Science and Technology, Rolla, MO, 65409

Nikhil Doiphode
Cummins Inc., Columbus, IN, 47201

Abstract

While cast iron is widely used in industry, a major limitation is the weldability of a dissimilar material onto cast iron due to hot cracking as a result of lack of ductility from graphite flakes. Consequently, a significant amount of preheat is often employed to reduce the cooling rate in the fusion zone, which, however, may lead to distortion of the welded parts. A potential remedy could be the Selective Laser Melting (SLM) process, where only small melt pools are created and thus the overall energy input is reduced. The present paper describes an investigation of the SLM process to join 304L stainless steel with cast iron. In this study, 304L stainless steel particles ranging from 15-45 μm in size were melted on a grey cast iron substrate by the SLM process. Multiple sets of parameter values were chosen to test different energy densities on the tensile strength of the bond created. Subsequent characterization of the bonded area included energy dispersive spectroscopy (EDS) mapping for obtaining insight into the elemental diffusion, and metallography for visualization of the microstructure. A range of energy densities was identified for purposes of eliminating bond delamination and maximizing mechanical strength.

Introduction

Selective Laser Melting (SLM) is an additive manufacturing process that utilizes a laser to melt metal powder particles in sequential layers to build three-dimensional parts modeled in Computer-Aided Design (CAD) software [1]. By melting the powder, SLM is capable of producing parts that approach theoretical density [2,3]. Due to the additive nature of the process, complex geometries can be produced that are otherwise impossible or impractical to create by conventional means. Therefore, SLM has attracted the interest of many companies including those in the aerospace and automotive industries. The parts made by SLM typically exhibit a high degree of dimensional accuracy no matter if they have complex geometries.

Cast iron normally contains between 2 – 4 % carbon content. One of the most common types of cast iron used in industry is grey cast iron. Grey cast iron can be identified by its graphite flakes, which are formed during the cooling process. It is largely used in industry because of its low cost, excellent machinability, and its ability to handle thermal cycling. However, among the different types of cast iron, grey cast iron is most susceptible to cracking due to its inherent brittleness as a consequence of graphite flakes present within the iron matrix [4]. Thus, grey cast

iron is often difficult to weld, which complicates bonding with dissimilar materials and repair to components that have been damaged [5].

One of the most common solutions that has been studied is to preheat the cast iron before welding [6–8]. Increasing the temperature of the cast iron decreases the amount of thermal shock experienced by the cast iron through a lowering of the cooling rate. As the part cools there are less residual stresses between the two dissimilar materials to cause cold cracking [9]. Typical preheat temperatures range from 300 – 600 °C, although care must be taken in order that the preheat does not cause distortion in the part [4]. If preheat cannot be used, then the use of nickel as a filler material for promotion of the austenitic phase is another possibility to produce successful welds. Nickel has a low coefficient of thermal expansion and therefore does not induce a significant amount of stress in the heat-affected zone (HAZ) of the weld, minimizing cracking [4,5]. As an extra precaution to avoid cracking, it is generally accepted that several small welds be made rather than one continuous weld to reduce residual stresses.

Although SLM often uses a continuous laser during fabrication, pulsed lasers are also available and provide the freedom to control the pulse shape for optimizing heat input [10]. Since a pulsed laser is in essence a series of small welds, it is conjectured that SLM using a pulsed laser may be suitable for welding grey cast iron than using a continuous laser. Furthermore, the flexibility SLM stemming from the ability to fine-tune laser process parameters allows for a wide range of possible energy input to weld cast iron. The research described in the present paper is part of an exploratory effort to evaluate SLM as a technique for welding grey cast iron to a dissimilar material, namely, 304L stainless steel. Several parameter sets are used for SLM of 304L onto grey cast iron as a means for adjusting the heat input for analysis of bond quality. The bond strength was tested through the use of tensile testing while the chemistry of the bonded area is provided through energy-dispersive spectroscopy (EDS) mapping.

Experimental Methods

A Renishaw AM250 SLM machine was used to melt and bond 304L stainless steel powder to a grey cast iron substrate. The AM250 contains a 200 W Nd-YAG pulsed laser with a Gaussian beam intensity profile and a spot size of approximately 70 μm. Before processing, the build chamber was inerted with argon gas until a stabilized oxygen content below 1000 ppm was observed. The inert atmosphere was maintained by keeping an overpressure of at least 5 mbar during fabrication within the build chamber and creating a sufficiently high argon flow rate across the build area of 400 ft^3/min. Furthermore, the substrate was heated to a temperature of 80 °C to improve the flowability of the powder while being spread across the build area and providing a slight preheat to reduce potential cracking of the cast iron and the bond area.

The powder used in this study was 304L stainless steel produced by LPW Technology using gas-atomization in an argon atmosphere. Figure 1 shows the SEM image of the as-received 304L powder, and the chemistry of the powder is given in Table 1. Using an ASPEX 1020 scanning electron microscope (SEM), the particle size distribution of the powder was measured using the projected areas of the particles for calculation of equivalent particle diameters. Cumulative distribution functions on both number and volume bases are shown in Figure 2. The D10, D50,

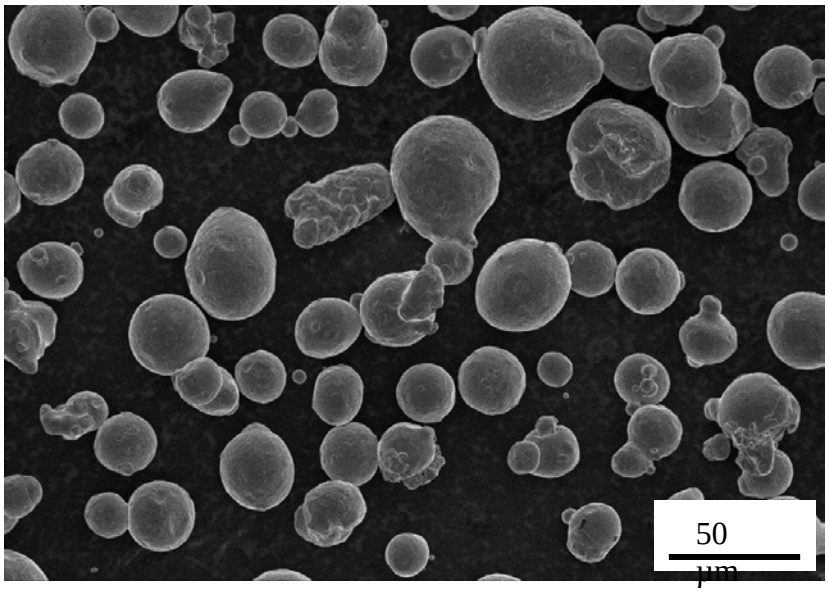

Figure 1: SEM image of as-received 304L powder processed by the Renishaw AM250.

and D90 values for both number and volume representations are given in Table 2, and they all fall within the 15 – 45 μm range specified by the powder supplier. Prior to being inserted into the Renishaw AM250, the virgin 304L powder was sieved through a 63 micron screen in an argon atmosphere to remove aggregates, large particles, and loosen agglomerates, as well as to minimize the amount of oxygen introduced into the build chamber.

Table 1: Chemical composition of virgin 304L stainless steel powder.

	Element										
	C	Cr	Cu	Fe	Mn	N	Ni	O	P	S	Si
Wt %	0.018	18.4	< 0.1	Bal	1.4	0.06	9.8	0.02	0.012	0.005	0.63

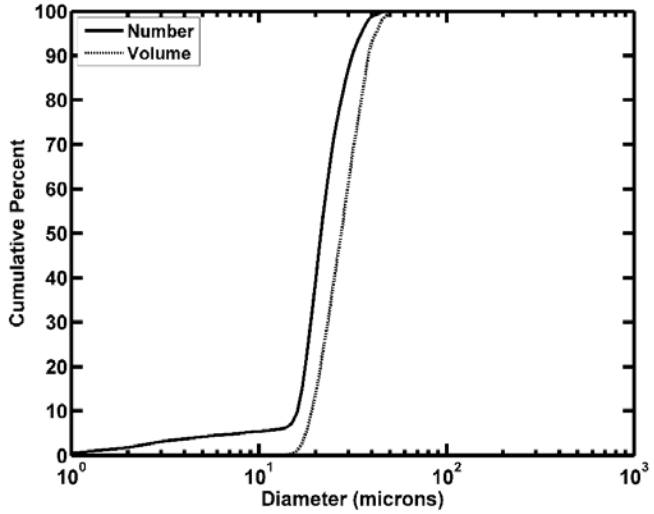

Figure 2: Number and volume size distributions of the 304L powder used in this study.

Table 2: A listing of the D10, D50, and D90 values pertaining to the measured size distributions of the 304L powder.

	Cumulative Distribution Results					
	Dn10	Dn50	Dn90	Dv10	Dv50	Dv90
Size (μm)	16.1	21.4	31.4	19.2	27.5	38.3

An illustration of the build layout is given in Figure 3a, where it can be seen that the cast iron substrate contains multiple protruding rectangular features, hereby referred to as protrusions. Starting with a solid piece of grey cast iron, a milling operation was performed to subtract all material except that which belongs to the protrusions. The rationale for introducing protrusions into the current study is twofold. By selectively melting the powder that is deposited on the protrusions, tensile specimens consisting of 304L and grey cast iron can be extracted with the bond location being at the center of the gage length without cutting into the build plate, as shown in Figure 2b. Moreover, incorporating protrusion features allowed for assessment of cracking. Since the SLM process induces residual stress in the melted material, any observed cracking should be noticeable at the edges of the protrusion rather than towards the center. In order to exacerbate this effect, the 100 mm length and 10 mm width of the protrusions was chosen, giving a length to width ratio of 10. In this light, if cracking is not observed at the edges, then the bond is deemed sufficient.

The dimensions of the tensile specimens used for evaluating bond strength are given in Figure 4. A Sodick VZ500LH wire EDM was utilized to precisely cut all specimens from the protrusions. Removal of possible oxidation induced during the EDM process was performed through mechanical polishing of the specimens with 600 SiC. All testing was conducted on an Instron UTM at a strain rate of 0.015 min^{-1} until 1% strain, whereby a strain rate of 0.5 min^{-1} was set. Although the relatively small size of the specimens may skew the yield strength, ultimate tensile strength, and elongation compared to that obtained with standard tensile bars, the purpose of this study is largely to assess the bond quality with respect to the location of failure in the gage length while comparing the tensile test results between the various laser parameters used.

All of the process parameters used are shown in Table 3, where each set is applied to a single protrusion. Since the Renishaw AM250 uses a pulsed laser, the distance between hatch scans, distance between successive pulses, and the duration of an individual laser pulse corresponding to the hatch spacing, point distance, and exposure time, respectively, must be defined. Combining all of these laser parameters in addition to the laser power and layer thickness allows for an estimation of energy density through the following equation:

$$\text{Energy Density} = \frac{(\text{Laser Power}) * (\text{Exposure Time})}{(\text{Hatch Spacing}) * (\text{Point Distance}) * (\text{Layer Thickness})}$$

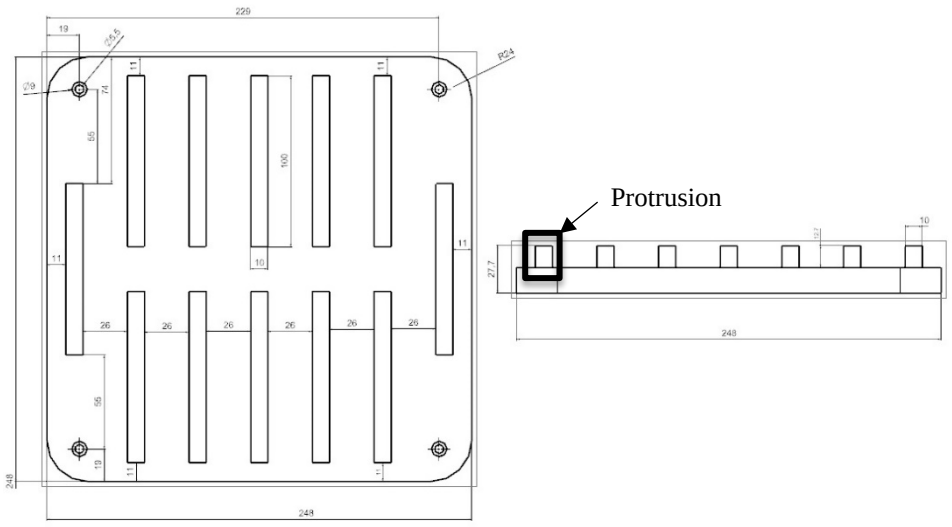

(a)

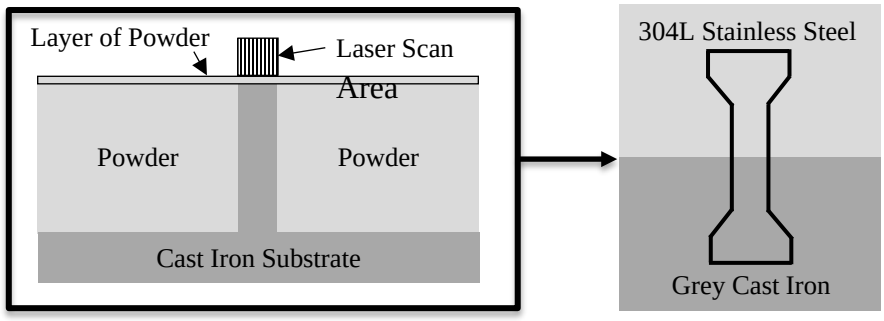

(b)

Figure 3: Illustration of the build layout showing (a) the geometry of the cast iron substrate with protrusions, and (b) the spreading of powder onto the cast iron for subsequent melting. Once the build is finished, the protrusions are removed and tensile specimens are cut with the bonding area being at the center of the gage length.

For this study, hatch spacing and laser power were varied to see this impact of both on the bond formed. Furthermore, the influence of energy density aids in the identification of process parameters needed for creating a strong and crack-free bond.

Broken tensile specimens from each parameter set were mounted in epoxy and polished to visualize the location at which failure occurred. Further characterization of the bonded area was done using a Hitachi S4700 SEM to collect EDS maps of the third parameter set in Table 3 for insight into the chemistry of the bonded area.

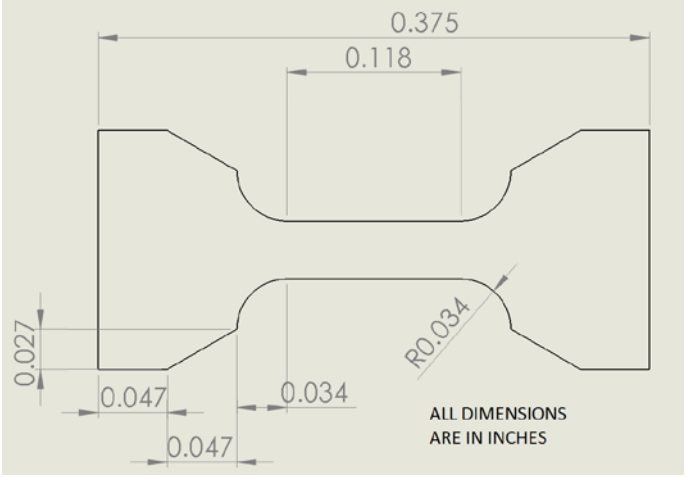

Figure 4: Dimensions of tensile specimens used for testing the bond strength between 304L stainless steel and grey cast iron.

Table 3: A listing of the parameter sets used where both the hatch spacing and laser power were altered independently to produce different energy densities.

	Parameter Set					
	1	2	3	4	5	6
Laser Power (W)	200	200	200	150	125	100
Hatch Spacing (µm)	45	65	85	85	85	85
Point Distance (µm)	60	60	60	60	60	60
Layer Thickness (µm)	50	50	50	50	50	50
Exposure Time (µs)	75	75	75	75	75	75
Energy Density (J/mm^3)	111	77	59	44	37	29

Results and Discussion

Parameter Sets 1 – 3: Hatch Spacing Variation

Figure 5 shows the results of varying the hatch spacing on the bond formed. In each of the parameter sets, cracking is observed at the ends of the protrusion. This is most likely due to the presence of residual stresses within the 304L material causing distortion. Residual stresses are inherent in the SLM part due to the rapid melting and solidification of the melt pool causing inhomogeneous material expansion and contraction. Kruth et al. [11] explained this phenomenon and mentions that the result of such a process causes parts to bend towards the laser beam. Since grey cast iron has low ductility as a consequence of graphite flakes present within the iron matrix, small distortions in the protrusion can lead to cracking. In order to study the location of the cracking, the ends of the protrusions were removed with a wire EDM, mounted, and polished. Optical micrographs of the cracking are also shown in Figure 5, and reveal that the cracks propagated either through the cast iron or along the bond area. For this reason, all of the tensile

specimens tested were cut from the center of the protrusion to assess the strength of the bond formed.

The tensile test results for the variation in hatch spacing are shown in Figure 6. Although the increase in hatch spacing seems to result in a higher UTS, the standard deviations in the measurements suggest that these differences are insignificant. In order to observe where failure occurred in the gage length, tensile specimens from each hatch spacing variation were mounted and polished. For all specimens observed, failure occurred well into the cast iron portion of the gage length and away from the bond. Figure 7 shows optical micrographs of the broken tensile specimens for each of the hatch spacings. Since all specimens failed within the cast iron, the insignificant UTS differences among the various hatch spacings tested are due to the variability in the cast iron. Therefore, the bond between 304L and grey cast iron is stronger than that of the cast iron. While the strength of the bond is greater than that of the cast iron, it is important to realize that the cracking at the edges of the protrusions implies that none of the hatch spacing parameter sets were completely successful.

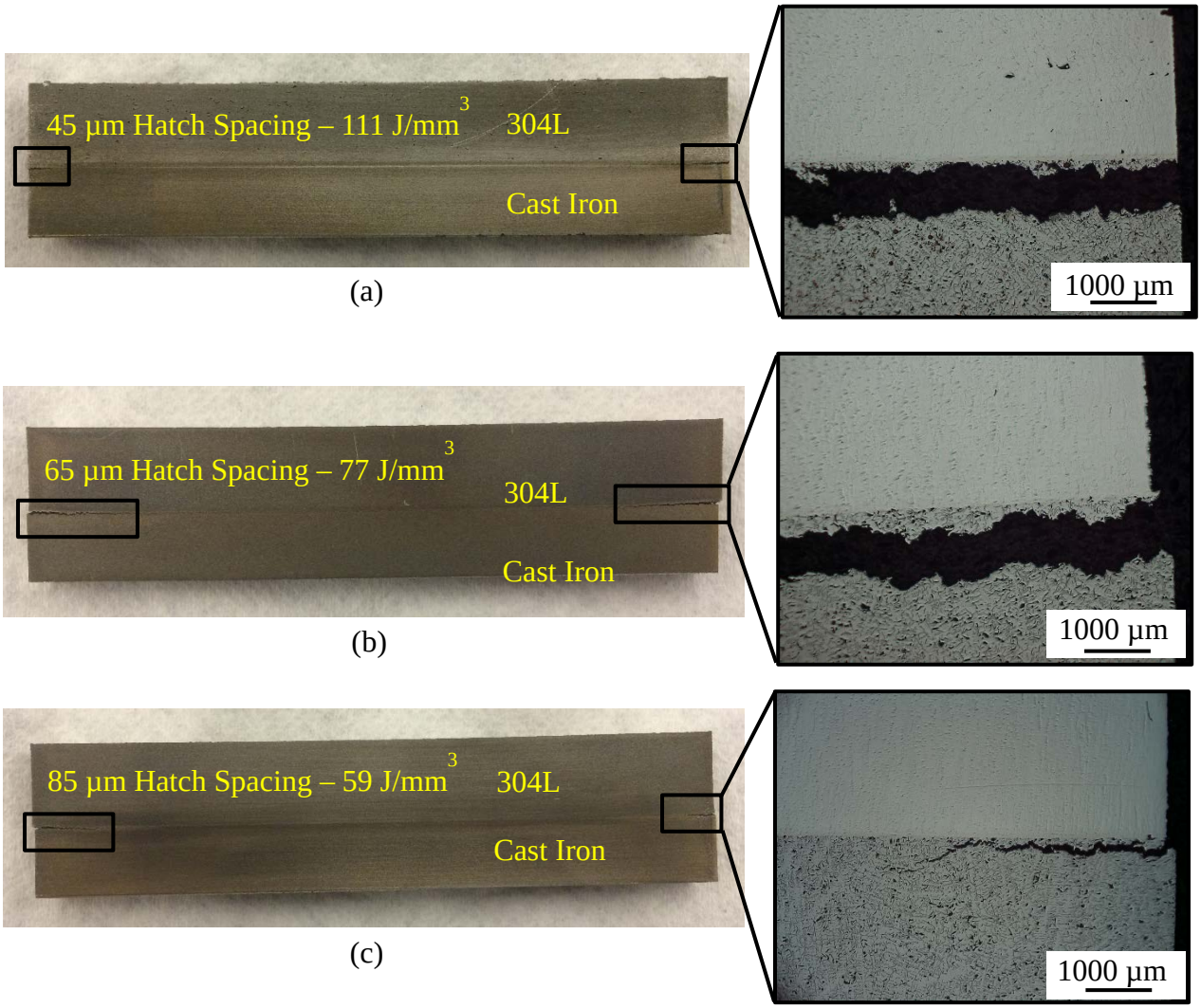

Figure 5: Images of the protrusions for various hatch spacings corresponding to the energy densities of (a) 111 J/mm^3, (b) 77 J/mm^3, and (c) 59 J/mm^3. Optical images of the edges of the protrusions show cracking in the cast iron and along the bond.

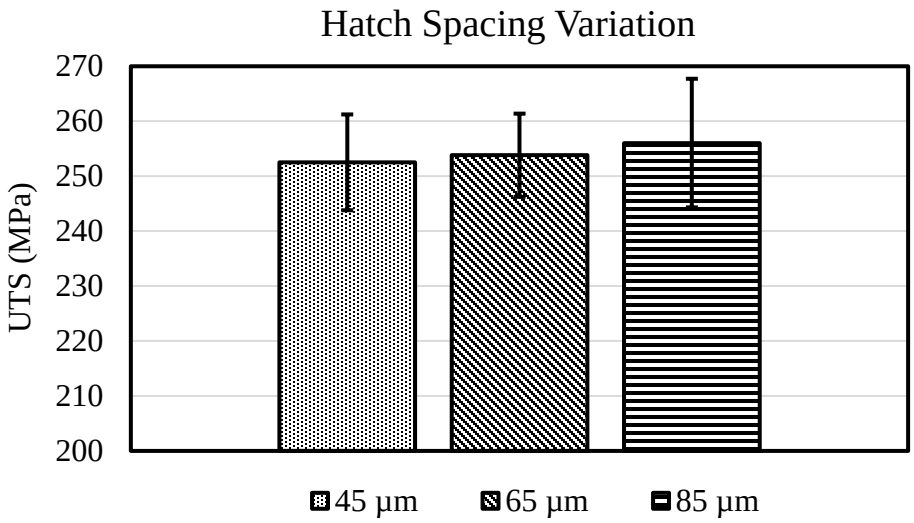

Figure 6: Tensile test data of all the hatch spacing variations illustrating no significant difference between the UTS among all energy densities.

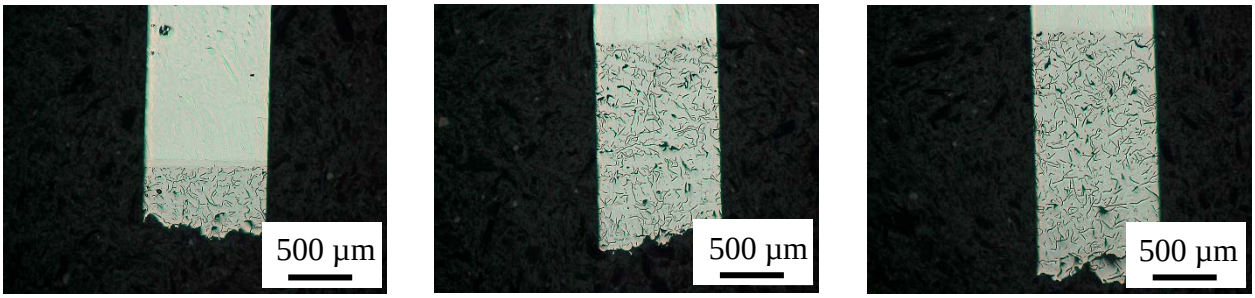

(a) (b) (c)

Figure 7: Optical micrograph of broken tensile specimens at a hatch spacing of (a) 45 µm, (b) 65 µm, and (c) 85 µm.

Parameter Sets 3 – 6: Laser Power Variation

Figure 8 shows the results of varying the laser power to obtain lower energy densities. Laser powers of 125 W and 150 W revealed only slight cracking at the edges of the protrusions unlike those found at the higher energy densities. This is attributed to the decrease in residual stresses as the energy density is lowered. In order to directly compare with the tensile results from parameter sets 1 – 3, all of the specimens were once again selected from the center.

At this point, it should be noted that a laser power of 100 W was not suitable for processing the 304L stainless steel powder due to the formation of undulations on the top surface of the protrusion (Figure 8a). There was no further processing using this parameter set in order to avoid damaging the recoating mechanism during the SLM operation. The bond strength formed by this parameter set could not be tested as there was not a sufficient amount of material to extract tensile

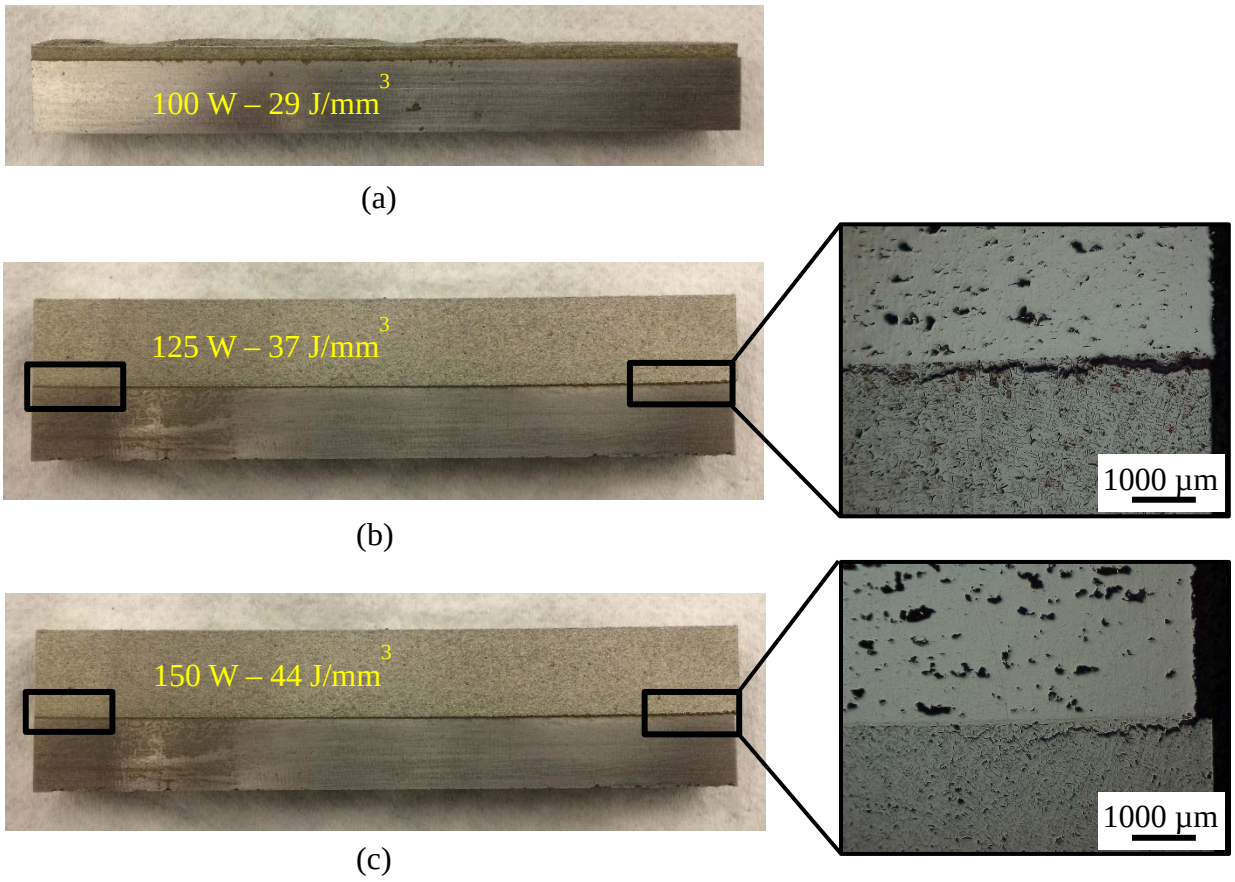

Figure 8: Images of the protrusions for various laser powers corresponding to the energy densities of (a) 29 J/mm^3, (b) 37 J/mm^3, and (c) 44 J/mm^3.

specimens. Using a wire EDM, a section of an undulation was removed from the protrusion, mounted, and polished. Figure 9 provides optical micrographs of said structure, and illustrates the high degree of porosity present. While no cracking is observed at the bonded area, it is apparent that a low laser power caused an insufficient amount of energy to melt the powder leading to a lack of fusion. It is unclear as to why the undulations form in particular regions, rather than across the entire length of the protrusion. Further studies need to be conducted to provide an explanation for this occurrence.

The tensile test results for the 125 W and 150 W laser powers are compared to that produced by 200 W mentioned previously. It is clear that a decrease in the laser power results in a lower UTS than that found at 200 W. Moreover, the standard deviations in the UTS values for the lower energy densities are also larger, meaning that more variability existed in the data. To explain this difference, broken tensile specimens were mounted and polished from both the 125 W and 150 W laser power. Figure 11 shows representative micrographs taken from the 125 W parameter set. Here it can be seen that the location of failure varied, where a few tests revealed the specimen

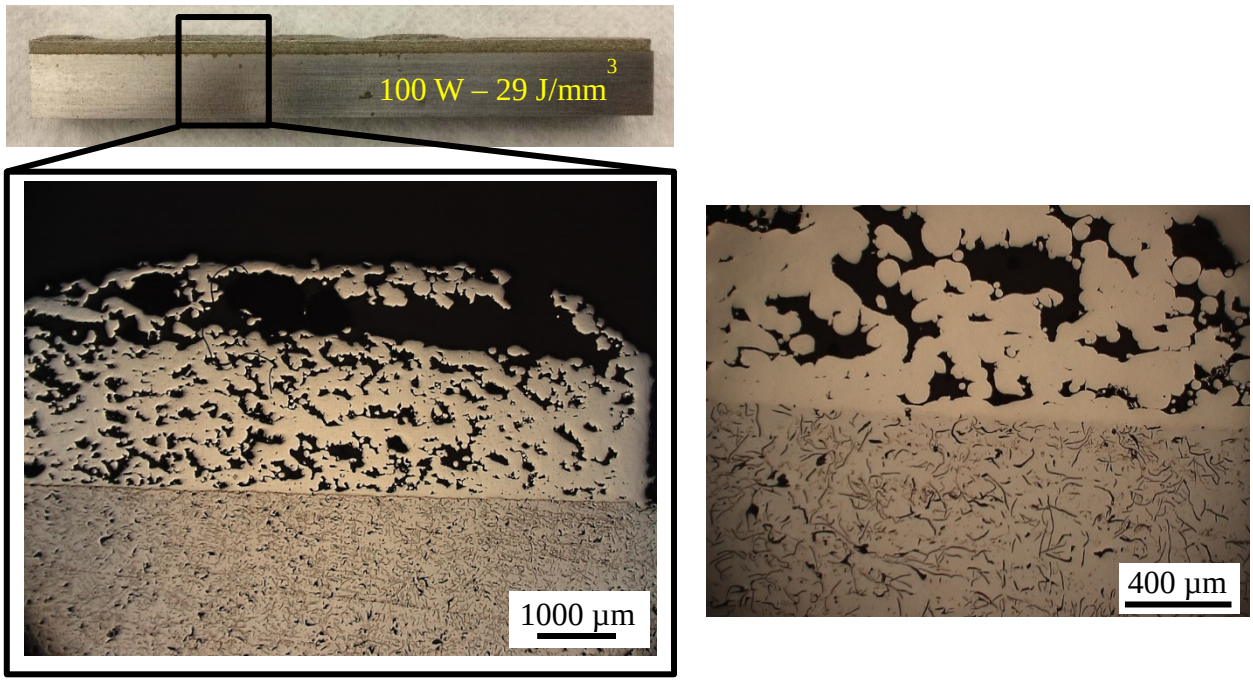

Figure 9: Optical micrographs showing the porosity in the 304L when at an energy density of 29 J/mm^3 corresponding to a laser power of 100 W.

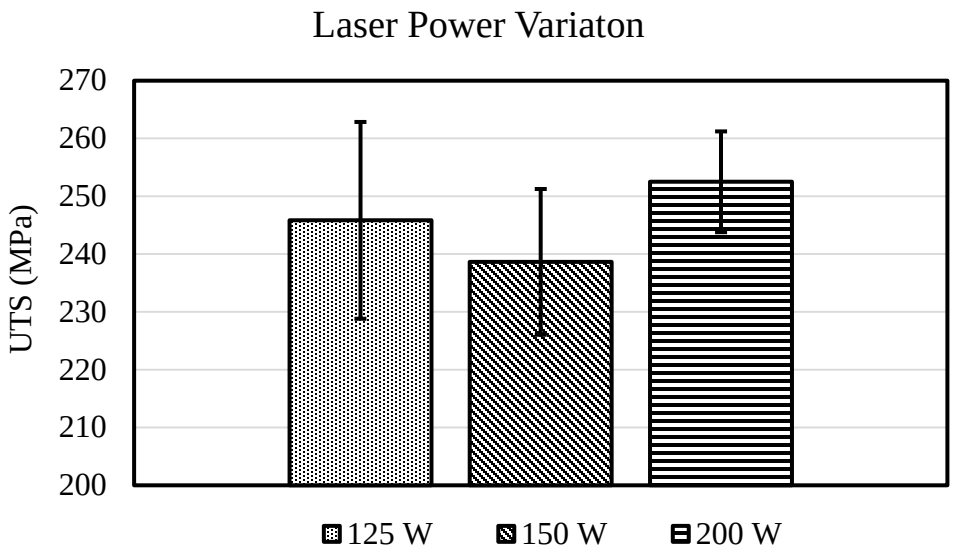

Figure 10: Tensile test data of all the laser power variations illustrating the increased variability in the data for the lower energy densities.

breaking in the 304L and others in the cast iron. This is due to the decrease in laser power where porosity in the stainless steel section made it rather weak. Therefore, the location of failure in these specimens was unpredictable and caused a large variation in the resulting UTS values. The same phenomenon was also noticed for the 150 W parameter set.

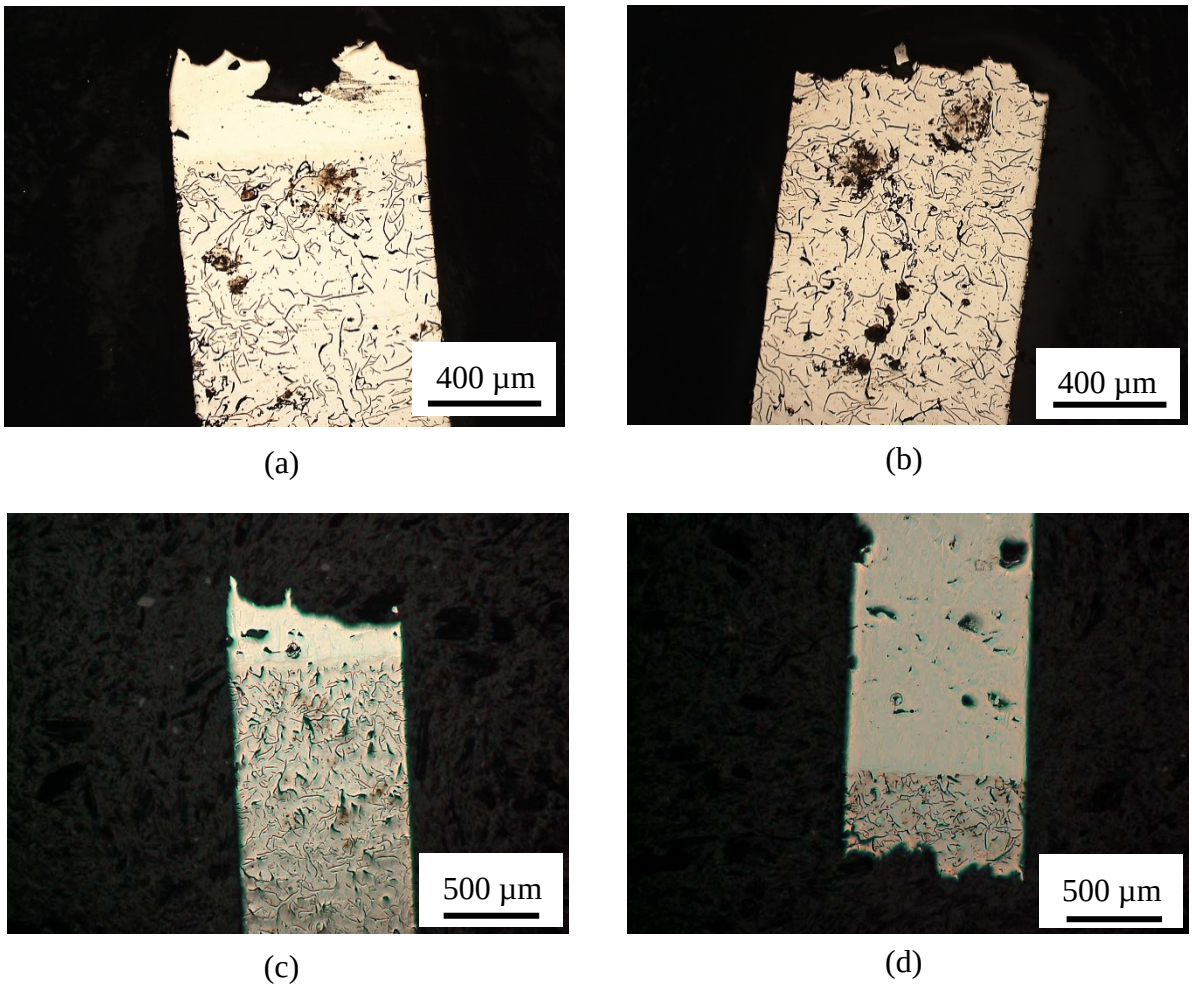

(a) (b)

(c) (d)

Figure 11: Optical micrographs for an energy density of 37 J/mm^3 and 44 J/mm^3 showing (a)(c) failure in the 304L and (b)(d) cast iron among different tensile specimens.

Although the lower energy densities showed an overall decrease in strength, it is important to note that in no case was their failure at the bond between the 304L and cast iron. It is also noteworthy that very little cracking was visible at the edges of the protrusions. This result indicates that the process parameters needed for a quality bond may not be able to produce dense 304L in the SLM process. As such, for the given substrate preheat, it may be necessary to grade the process parameters from the bond area to those required to fabricate dense 304L.

Distribution of Chemical Elements at Bond Area

Although the two materials being bonded in this study contain an iron matrix, the chemistry of each is significantly different from the other as a result of alloying additions. While 304L contains high chromium to create a protective oxide layer and a large amount of nickel to stabilize the austenitic phase to room temperature, grey cast iron contains little to no chromium or nickel. Instead, grey cast iron contains silicon, manganese, and a high carbon concentration in the form of graphite flakes. This large difference in chemical composition can possibly lead to diffusion of

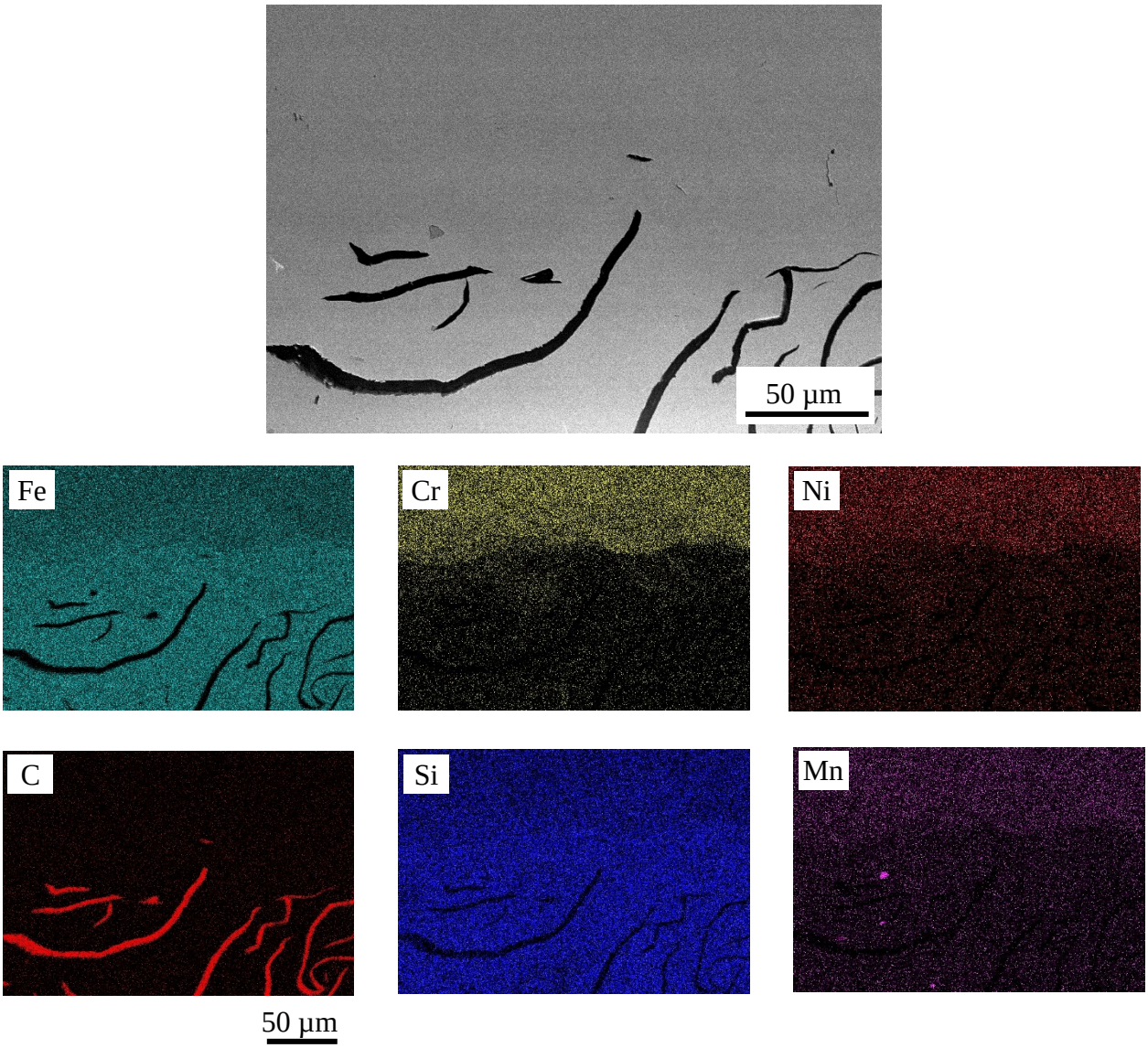

Figure 12: EDS mapping of chemical species at bond area for a laser power of 200 W and hatch spacing of 85 µm.

elements at the bond from one material to the other, causing the formation of various brittle phases including iron carbide, chromium carbide, and nickel carbide.

Figure 12 shows the results from the EDS mapping performed on parameter set 3 with an energy density of 59 J/mm^3. Carbon diffusion from the base metal into the bond area is not visible based on the data collected. It is possible that carbon diffused, but only in trace amounts due to the rapid solidification inherent in SLM. A high cooling rate coupled with the possibility of carbon diffusion into the austenitic 304L leads to the possibility of martensite forming at the bond area. Due to the brittle nature of martensite, such a phase is not desired in welding as cracking can often result. Therefore, in addition to understanding the chemistry at the bond, it is highly beneficial to reveal its microstructure for insight into any deleterious phases that can cause failure at the weld location.

Another interesting observation of the bond area is the presence of chromium and nickel where the concentrations of each appear to be less than that in the 304L. This indicates that mixing of 304L and cast iron is occurring at the bond. The use of nickel in bonding cast iron has been shown to serve as an effective means for welding cast iron since it has a low coefficient of thermal expansion. Thus, residual stresses in the weldment are minimized eliminating cracking in the HAZ even when the fusion zone expands and contracts due to melting and solidification [4]. Therefore, the high percentage of nickel in 304L will its weldability to grey cast iron. This could explain why there were no cracks observed along the bond at the center of the protrusions.

Conclusions

In this study, an SLM process utilizing a pulsed laser beam was investigated as a means for additive fabrication of 304L onto a grey cast iron substrate. The SLM machine used utilizes a pulsed laser beam. Since the SLM process allows flexibility for adjusting the energy input at the melt pool as a function of laser parameters, the experiments performed tested various energy densities to find the parameters toward creating a quality bond between the two materials.

While a bond stronger than the cast iron substrate was found, it was also found that energy densities greater than 59 J/mm^3 led to cracking at the ends of the cast iron protrusions. This result suggested that the residual stress induced in the 304L was large enough to cause the brittle cast iron to crack. On the contrary, all energy densities below 59 J/mm^3 revealed very little cracking, even at the protrusion edges. However, these parameters proved to be non-optimal for the fabrication of 304L onto the grey cast iron substrate where a significant amount of porosity was observed in the fabricated 304L. Consequently, the variability in the tensile test data increased since failure could occur in either the 304L or the cast iron material. It is therefore concluded that the process parameters necessary for producing a quality bond are different from that for fabricating dense 304L. This indicates that the laser parameters may need to be graded from the bond area to the 304L in order to have both a strong bond and dense 304L.

EDS mapping of the bond area showed that the two materials are chemically mixing due to their differences in chromium and nickel concentrations. This will undoubtedly alter the solidification and kinetics of the phases formed at the bond. While no carbon diffusion was detected, further observation will be needed in order to confirm this result. Such an analysis will allow more insight into the possible formation of brittle carbide phases.

Acknowledgements

This research is sponsored by the Industrial Consortium of the Center for Aerospace Manufacturing Technologies (CAMT) at Missouri University of Science and Technology.

References

[1] A.T. Sutton, C.S. Kriewall, M.C. Leu, J.W. Newkirk, Powder characterisation techniques and effects of powder characteristics on part properties in powder-bed fusion processes, Virtual Phys. Prototyp. 12 (2016) 3–29. doi:10.1080/17452759.2016.1250605.

[2] J.P. Kruth, G. Levy, F. Klocke, T.H.C. Childs, Consolidation phenomena in laser and

powder-bed based layered manufacturing, CIRP Ann. - Manuf. Technol. 56 (2007) 730–759. doi:10.1016/j.cirp.2007.10.004.
[3] N. Guo, M.C. Leu, Additive manufacturing: Technology, applications and research needs, Front. Mech. Eng. 8 (2013) 215–243. doi:10.1007/s11465-013-0248-8.
[4] M. Pouranvari, On the weldability of grey cast iron using nickel based filler metal, Mater. Des. 31 (2010) 3253–3258. doi:10.1016/j.matdes.2010.02.034.
[5] J. Bennett, R. Dudas, J. Cao, K. Ehmann, G. Hyatt, Control of heating and cooling for direct laser deposition repair of cast iron components, Int. Symp. Flex. Autom. ISFA 2016. (2016) 229–236. doi:10.1109/ISFA.2016.7790166.
[6] M. Nakamura, Y. Sawada, Y.S. Sato, Metallographic Study of Lapped FSW between Ductile Cast Iron and Austenite Type Stainless Steel, Mater. Sci. Forum. 638–642 (2010) 1197–1202. doi:10.4028/www.scientific.net/MSF.638-642.1197.
[7] E.M. El-Banna, Effect of preheat on welding of ductile cast iron, Mater. Lett. 41 (1999) 20–26.
[8] R. Jendrzejewski, G. Śliwiński, M. Krawczuk, W. Ostachowicz, Temperature and stress during laser cladding of double-layer coatings, Surf. Coatings Technol. 201 (2006) 3328–3334. doi:10.1016/j.surfcoat.2006.07.065.
[9] J.M. Pelletier, J.M.P. and A.B.V. annes M. Pilloz, Residual stresses induced by laser coatings : phenomenological analysis and predictions, J. Mater. Sci. 27 (1992) 1240 – 1244.
[10] K. a. Mumtaz, N. Hopkinson, Selective Laser Melting of thin wall parts using pulse shaping, J. Mater. Process. Technol. 210 (2010) 279–287. doi:10.1016/j.jmatprotec.2009.09.011.
[11] J.P. Kruth, L. Froyen, J. Van Vaerenbergh, P. Mercelis, M. Rombouts, B. Lauwers, Selective laser melting of iron-based powder, in: J. Mater. Process. Technol., 2004: pp. 616–622. doi:10.1016/j.jmatprotec.2003.11.051.
[12] J.W. Fu, Y.S. Yang, J.J. Guo, W.H. Tong, Effect of cooling rate on solidification microstructures in AISI 304 stainless steel, Mater. Sci. Technol. 24 (2008) 941–944. doi:10.1179/174328408X295962.